





# Enhancement of zero-field skyrmion density in [Pt/Co/Fe/Ir]<sub>2</sub> multilayers at room temperature by the first-order reversal curve

Cite as: J. Appl. Phys. **127**, 223901 (2020); <https://doi.org/10.1063/5.0004432>

Submitted: 14 February 2020 . Accepted: 22 May 2020 . Published Online: 08 June 2020

Mangyuan Ma, Calvin Ching Ian Ang , Yong Li, Zizhao Pan, Weiliang Gan , Wen Siang Lew , and Fusheng Ma 



View Online



Export Citation



CrossMark

Lock-in Amplifiers  
up to 600 MHz







# Enhancement of zero-field skyrmion density in [Pt/Co/Fe/Ir]<sub>2</sub> multilayers at room temperature by the first-order reversal curve

Cite as: J. Appl. Phys. 127, 223901 (2020); doi: 10.1063/5.0004432

Submitted: 14 February 2020 · Accepted: 22 May 2020 ·

Published Online: 8 June 2020



Mangyuan Ma,<sup>1</sup> Calvin Ching Ian Ang,<sup>2</sup>  Yong Li,<sup>1</sup> Zizhao Pan,<sup>1</sup> Weiliang Gan,<sup>2</sup>  Wen Siang Lew,<sup>2,a)</sup>   
and Fusheng Ma<sup>1,a)</sup> 

## AFFILIATIONS

<sup>1</sup>Jiangsu Key Laboratory of Opto-Electronic Technology, Center for Quantum Transport and Thermal Energy Science, School of Physics and Technology, Nanjing Normal University, Nanjing 210046, China

<sup>2</sup>School of Physical and Mathematical Sciences, Nanyang Technological University, 21 Nanyang Link, 637371 Singapore

<sup>a)</sup>Authors to whom correspondence should be addressed: [phymafs@njnu.edu.cn](mailto:phymafs@njnu.edu.cn) and [wensiang@ntu.edu.sg](mailto:wensiang@ntu.edu.sg)

## ABSTRACT

Magnetic skyrmions are novel topological spin textures on the nanoscale, and significant efforts have been taken to improve their zero-field density at room temperature (RT). In this work, we reported an approach of improving zero-field skyrmion density in [Pt/Co/Fe/Ir]<sub>2</sub> multilayers at RT by using the first-order reversal curve (FORC) technique to obtain information on the irreversible or reversible behaviors in the magnetization switching process. It was found from the FORC diagram that the magnetization reversal mechanism can be characterized into three stages: (1) reversible labyrinth stripe domains expanding or shrinking stage; (2) irreversible stripe domains fracturing stage; and (3) irreversible skyrmion annihilation stage. Furthermore, the zero-field skyrmion density can be highly improved by choosing reversal fields from the irreversible stripe domains fracturing stage. The highest skyrmion density was approached according to the maximum FORC distribution  $\rho$ . Our results have established the FORC measurement as a valuable tool for investigating magnetic multilayers of high skyrmion densities.

Published under license by AIP Publishing. <https://doi.org/10.1063/5.0004432>

## I. INTRODUCTION

Magnetic skyrmions are topologically protected quasi-particles with non-trivial spin texture which could serve as information carriers in novel spintronic devices, such as magnetic racetrack memory, logic gates, spin-torque oscillators, and artificial synapses/neurons.<sup>1–5</sup> In recent years, the existence of skyrmions in magnet/heavy-metal multilayers with perpendicular magnetic anisotropy at room temperature (RT) has been realized resulting from the competition between Dzyaloshinskii–Moriya interaction (DMI), dipolar interaction, and exchange interaction.<sup>6–10</sup> However, it is still challenging to approach high skyrmion densities without the assistance of an external magnetic field at RT. To overcome this obstacle, lots of work have been done,<sup>11–17</sup> for instance, generating high density skyrmions from the labyrinth domains at zero-field in Pt/Co/Ta multilayers using an electromagnetic coordinated method<sup>14</sup> and a scanning local magnetic field.<sup>16</sup>

The first-order reversal curve (FORC) technique has been proven to be an effective method in probing the magnetization reversal mechanism.<sup>18–27</sup> This approach collects a larger dataset compared with the complete magnetization hysteresis ( $M$ - $H$ ) loop, from which information about the distribution of switching fields and interaction fields for all of the domains that contribute to the  $M$ - $H$  loop and the irreversibility of magnetization switching can be derived, such as the magnetization switching process during complete reversal in Co/Pt multilayers.<sup>28</sup> An open question is that whether the zero-field skyrmion density can be highly improved via analyzing the process of magnetization reversal or not. A thorough understanding of the magnetization switching processes involved in skyrmion-hosting materials must first be obtained.

In this work, we demonstrated a mechanism for improving zero-field skyrmion density in [Pt/Co/Fe/Ir]<sub>2</sub> multilayers at RT by using the FORC technique. The magnetization switching process

displays a distinctive characteristic of irreversible and reversible behaviors from the FORC diagram. By increasing the field from zero to saturation, a predominant reversible behavior is first observed due to the labyrinth stripe domains expanding or shrinking in width without changing their topology. As the field increases, the stripe domains irreversibly fracture into multiple skyrmions. Finally, the skyrmions annihilate irreversibly approaching saturation. It is found that the zero-field skyrmion density is higher by choosing a reversal field from the irreversible stage than the reversible stage. The highest skyrmion density was achieved from the reversal field corresponding to the maximum FORC distribution value. Our findings are of great significance for the successful application of skyrmions for practical applications.

## II. EXPERIMENTAL METHOD

The multilayer film stack of Ta(5)/Ir(2)/[Pt(1)/Co(0.5)/Fe(0.4)/Ir(0.9)]<sub>2</sub>/Ta(2) (the numbers in parentheses are the nominal layer thickness in nanometer) was deposited on a thermally oxidized silicon wafer using direct current magnetron sputtering techniques at RT. A base pressure of  $1 \times 10^{-7}$  Torr or better is reached before sputtering is initiated. Argon gas was used during the sputtering process at 2.0 mTorr for all materials except Co that was sputtered at 3.0 mTorr. The deposition rates for Ta, Pt, Co, Fe, and Ir were 0.62, 0.68, 0.26, 0.30, and 0.37 Å/s, respectively. The bottom Ta layer was used as an amorphous and adhesive underlayer. The additional Ir underlayer was added to provide a similar interface for the repeating layers. Additional capping layer of Ta was used as a protective layer against oxidation.

The out-of-plane  $M$ - $H$  loop and FORCs of the [Pt/Co/Fe/Ir]<sub>2</sub> multilayers were measured by the MagVision Kerr microscopy system in the polar mode with magnetization imaged simultaneously. To remove the non-magnetic background signal, differential imaging was performed. Due to the longer measurement durations needed for FORC, piezo-motors were used to compensate for the sample drift.

## III. RESULTS

A full  $M$ - $H$  loop under an out-of-plane magnetic field  $H_z$  was first measured using the polar magneto-optical Kerr effect (MOKE) at RT as shown in Fig. 1. The red and blue solid lines represent the ascending and descending branches, respectively. The insets show the MOKE images that correspond to the out-of-plane magnetization configurations at selected fields. The whole magnetization reversal process can be understood from the variation of the magnetic domain configurations. As the ascending and descending branches are symmetrical, we will explain the variation of magnetic domains along the ascending branch. We divide the process into polarized (from  $-20$  to  $0$  Oe) and un-polarized (from  $0$  to  $20$  Oe) parts. In the polarized part, starting from the negatively saturated state as shown in image 1, the magnetic domain configurations gradually transfer to complex domains of long labyrinth stripes. First, certain regions of the [Pt/Co/Fe/Ir]<sub>2</sub> multilayers usually containing defects lower the energy barrier for magnetization reversal. These regions will be reversed in the form of circular domains, i.e., the presence of magnetic skyrmions (image 2), as a result of the competition between DMI and demagnetizations.<sup>29–31</sup> The

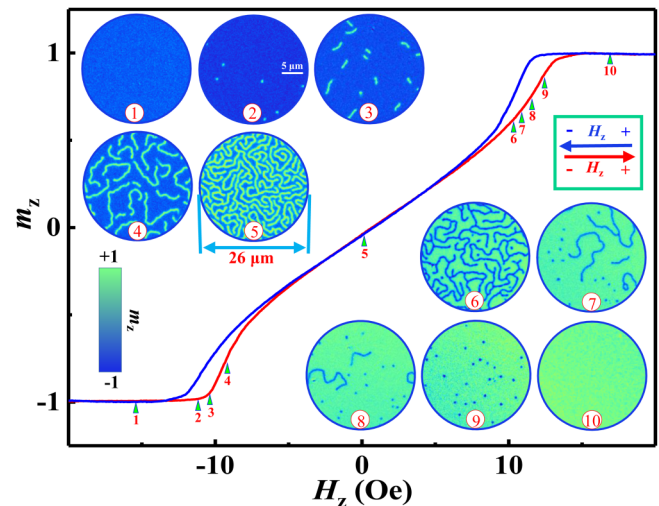


**FIG. 1.** Evolution of the out-of-plane magnetization configurations in [Pt/Co/Fe/Ir]<sub>2</sub> multilayers at RT. The red and blue solid lines represent the ascending and descending branches of the  $M$ - $H$  loop, respectively. Insets are differential polar-MOKE images showing the field evolution of magnetic domains at selected fields as labeled by triangles along the ascending branch of the  $M$ - $H$  loop. A circular region with a diameter of  $26 \mu\text{m}$  was prepared from the measured Kerr images.

estimated diameter of skyrmions in image 2 is about  $400\sim 500$  nm. Second, these skyrmion-like domains expand in a non-symmetrical manner and become into short labyrinth stripes with increasing  $H_z$  (image 3). After that, the short stripes lengthen continuously in random directions (image 4) and reach an up/down magnetization balanced remanent configuration at zero field (image 5). In the un-polarized part, the magnetic domains change roughly in an inverse process of the aforementioned process. The long stripes first shorten with the field increases from zero and approach a complex configuration comprised of both stripes and skyrmions (image 6). Then, the stripes continuously shrink and also break into skyrmions simultaneously, and the changes become more obvious with increasing external field (images 7 and 8). Image 9 shows a pure skyrmion configuration with all the stripes disappear. Finally, the skyrmions gradually annihilated and a positively saturated state arrives when the field is larger than  $15$  Oe (image 10). To be noted is that there is hardly any skyrmions in the magnetization configuration at zero-field as shown in image 5 of Fig. 1. As shown in Fig. 1, the skyrmions in image 2 spontaneously nucleate, while the skyrmions in image 9 result from the breakup of the labyrinth domains. The different skyrmion formation mechanisms decide the skyrmion densities, and the skyrmion density in image 9 is much larger than that in image 2. An open question is that whether the zero-field skyrmion density can be enhanced if we reverse field from a non-saturation field to zero field. To verify this assumption, we adopt the FORC measurement to analyze the irreversible or reversible behaviors in the magnetization switching process.

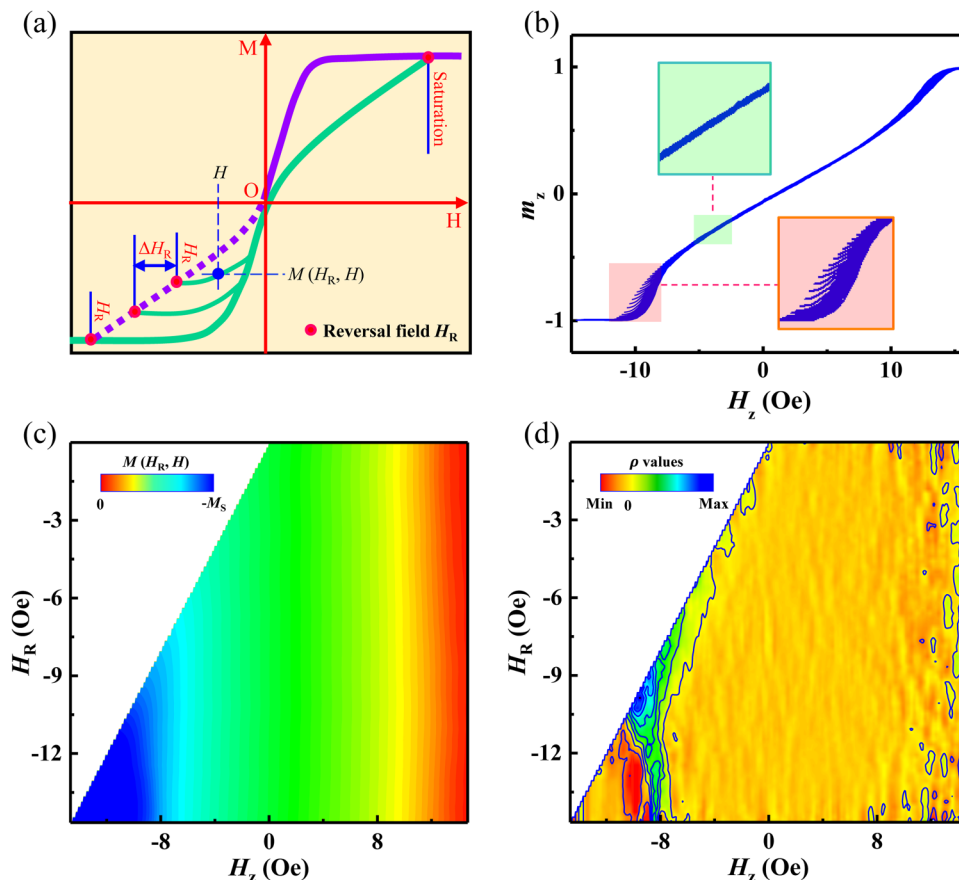
To improve the skyrmion density at zero-field, the FORC technique was adopted to investigate the magnetization reversal characteristics of the  $[\text{Pt}/\text{Co}/\text{Fe}/\text{Ir}]_2$  multilayers, in particular, the details of the reversible and irreversible behaviors of the magnetization switching process with the history of the field  $H_z$ . The FORC measurement can be carried out along both the ascending branch and the descending branch of the  $M$ - $H$  loop.<sup>32</sup> In view of the symmetrical reversal processes along the two branches, in this work, we did the FORC measurement in the manner as defined in Fig. 2(a). First, a positive field of  $H_{\text{sat}}$ , large enough to saturate the sample, was applied, and then  $H_z$  decreases to the selected fields of  $H_R$  [red dots in Fig. 2(a)], from which the field increases to  $H_{\text{sat}}$ . These minor  $H_{\text{sat}}-H_R-H_{\text{sat}}$   $M$ - $H$  loops form the whole FORCs together. Figure 2(b) shows the measured FORCs with the reversal fields  $H_R$  selected in a constant interval of 3 Oe, in which the outer boundary delineates the major  $M$ - $H$  loop.<sup>33-35</sup> The insets show the zoomed-in views of two portions of the FORCs, which indicate the reversible and irreversible regions of magnetization. To better understand the minor  $H_{\text{sat}}-H_R-H_{\text{sat}}$   $M$ - $H$  loops, the FORCs are usually analyzed by a corresponding FORC diagram. The magnetization can be traced out from the FORCs of Fig. 2(b) as a two-variable function  $M(H_R, H_z)$  in the  $(H_R, H_z)$  plane as shown in Fig. 2(c). The FORC distribution

function, a FORC diagram, can be calculated by<sup>20,34,37,38</sup>

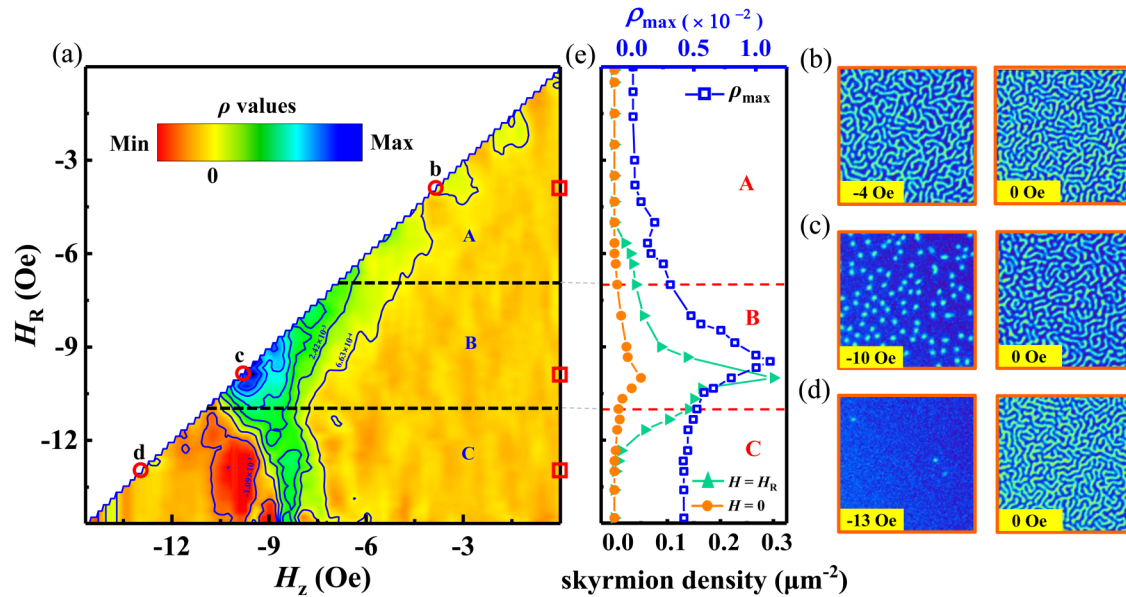
$$\rho = -\frac{1}{2} \frac{\partial^2 M(H_R, H_z)}{\partial H_R \partial H_z} dH_z. \quad (1)$$

Figure 2(d) is the contour map plotting of  $\rho$ .<sup>32</sup>

The FORC diagram reveals the occurrence of reversible and irreversible changes in the reversal process:  $\rho=0$  for the pure reversible changes, while  $\rho \neq 0$  for irreversible changes.<sup>28,32,39</sup> To understand the reversible and irreversible switching processes, we mainly focused on the third quadrant of the FORCs diagram since the selected reversal fields  $H_R < 0$ . According to the values of  $\rho$  in Fig. 3(a), we divide the FORC diagram into three regions as marked by A, B, and C, respectively. Region A ( $0 \text{ Oe} \leq -H_R \leq 7 \text{ Oe}$ ) is a nearly featureless region with the value of  $\rho$  close to zero. Here, the value of  $\rho$  is nearly zero and which implies a reversible magnetization change corresponding to the FORCs as the top inset in Fig. 2(b). The magnetization reversal processes are reversible with the width of the stripe domains shrinking with field  $H_z$  and the number of domains keeping unchanged. In contrast, in region B ( $7 \text{ Oe} \leq -H_R \leq 11 \text{ Oe}$ ), the value of  $\rho$  changes highly with the presence of a maximum at  $(-H_R, -H_z) = (9.6 \text{ Oe}, 9.6 \text{ Oe})$ . The field-dependent variation of  $\rho$  indicates the existence of an



**FIG. 2.** FORC measurement and magnetization irreversibility. (a) Schematic of FORC measurement: the red dots represent magnetizations at the reversal fields  $H_R$ , the green solid lines represent the field sweeping paths, and  $\Delta H_R$  represents an interval between reversal fields of 3 Oe. (b) Polar-MOKE measured FORCs of  $[\text{Pt}/\text{Co}/\text{Fe}/\text{Ir}]_2$  multilayers. Insets are zoomed-in views of different portions of FORCs. (c) 2D map of magnetization values obtained by measuring magnetization along each FORC. (d) FORC diagram, a contour plot of the corresponding FORC distribution  $\rho$ .



**FIG. 3.** Magnetization reversibility and irreversibility characterized by domain topology modification. (a) FORC diagram divided into three regions according to the degree of reversible or irreversible behaviors. (b)–(d) Polar-MOKE images (the side length is  $20 \mu\text{m}$ ) of the magnetic domain structures measured at selected reversal fields  $H_R = -4$ ,  $-10$ , and  $-13$  Oe corresponding to aforementioned three regions [left column, open circles in (a)] and subsequently measured at the corresponding remanent states [right column, open squares in (a)]. (e) Skyrmion density measured at selected reversal fields  $H_R$  (green solid line with symbols of triangles) and subsequently measured at the remanent states when field changed from  $H_R$  to 0 (origin solid line with symbols of dots). The maximum values of the FORC distribution  $\rho$  measured at different reversal fields represented by the blue solid line with symbols of open squares.

irreversible behavior during magnetization switching, which corresponds to a non-overlapped part of the FORCs as the bottom inset in Fig. 2(b). The irreversible process corresponds to the fission of stripe domains into skyrmions. Finally, in region C ( $11 \text{ Oe} \leq -H_R \leq 15 \text{ Oe}$ ), the  $H_R$  close to the negative saturation field, a variation of  $\rho$  was observed with the presence of a negative valley and a positive peak at  $H = -10.0$  and  $-8.5$  Oe, respectively. The pair of negative–positive peaks indicates the annihilation of skyrmions.

We measured polar-MOKE images of the magnetic domain structures at three reversal fields  $H_R = -4$ ,  $-10$ , and  $-13$  Oe as shown in the left column of Figs. 3(b)–3(d). The three  $H_R$  were selected from the aforementioned three regions. The images of the magnetic domains at the corresponding remanent states by increasing the external fields from  $H_R$  to zero are shown in the right column of Figs. 3(b)–3(d), respectively. It is found that the number of skyrmion at  $H_R$  located in region B is much larger than that at  $H_R$  in regions A and C. In the meanwhile, the number of skyrmion at the remanent state corresponding to  $H_R$  located in region B is also higher than that corresponding to  $H_R$  located in regions A and C.

The dependence of skyrmion densities at  $H_z = H_R$  and  $H_z = 0$  on  $H_R$  is plotted in Fig. 3(e); the skyrmion density is defined as the counted skyrmion numbers divided by the image area. It is found that the zero-field skyrmion density first increases when the  $H_R$  increases from region A to B and approaches a maximum value of  $0.05 \mu\text{m}^{-2}$  where the skyrmion density at the corresponding  $H_R$  are

also the largest. Then, the zero-field skyrmion density decreases with the  $H_R$  increasing from region B to C. To further correlate the degree of irreversibility quantified by  $\rho$  from the FORC diagram with the enhancement of zero-field skyrmion densities, i.e., first increasing to a maximum value in region B and then decreasing from there when the  $H_R$  increases from region B to C. Furthermore, the maximum value of the  $\rho_{\text{max}}$  and the zero-field skyrmion density appears at a very similar  $H_R$ . Therefore, the improvement of zero-field skyrmion density can be directly correlated to the maximum  $\rho$  value in the FORC diagram. To maximize the zero-field skyrmion density, we can choose a reversal field  $H_R$  corresponding to the maximum value of  $\rho$  in the  $H_{\text{sat}}-H_R=0$  process.

#### IV. CONCLUSION

In summary, our MOKE and FORC measurements reveal three distinct magnetization switching mechanisms in  $[\text{Pt}/\text{Co}/\text{Fe}/\text{Ir}]_2$  multilayers: (1) reversible stripe domains expanding and shrinking; (2) irreversible fission of stripe domains into skyrmions; and (3) irreversible skyrmions annihilation. We have found an effective method to improve the zero-field skyrmion density using the FORC technique: the skyrmion density at remnant can be highly enhanced by choosing the reversal fields corresponding to

high FORC distribution  $\rho$  values. Therefore, the FORC technique is an effective method for skyrmionic application at zero field.

### AUTHORS' CONTRIBUTION

M.M. and C.C.I.A. contributed equally to this work.

### ACKNOWLEDGMENTS

Work performed at the Nanjing Normal University was supported by the National Natural Science Foundation of China (NNSFC; Grant No. 11704191), the Natural Science Foundation of Jiangsu Province of China (Grant No. BK20171026), the Jiangsu Specially-Appointed Professor, and the Six-Talent Peaks Project in Jiangsu Province of China (Grant No. XYDXX-038). Work performed at the Nanyang Technological University was supported by a NRF-CRP Grant (No. CRP9-2011-01), a RIE2020 ASTAR AME IAF-ICP Grant (No. I1801E0030), and an ASTAR AME Programmatic Grant (No. A1687b0033). W.S.L is a member of the SG-SPIN Consortium.

### DATA AVAILABILITY

The data that support the findings of this study are available from the corresponding author upon reasonable request.

### REFERENCES

- <sup>1</sup>A. Fert, V. Cros, and J. Sampaio, "Skyrmions on the track," *Nat. Nanotechnol.* **8**, 152–156 (2013).
- <sup>2</sup>R. Tomasello, E. Martinez, R. Zivieri, L. Torres, M. Carpentieri, and G. Finocchio, "A strategy for the design of skyrmion racetrack memories," *Sci. Rep.* **4**, 6784 (2014).
- <sup>3</sup>X. Zhang, G. P. Zhao, H. Fangohr, J. P. Liu, W. X. Xia, J. Xia, and F. J. Morvan, "Skyrmion-skyrmion and skyrmion-edge repulsions in skyrmion-based racetrack memory," *Sci. Rep.* **5**, 7643 (2015).
- <sup>4</sup>W. Kang, Y. Huang, C. Zheng, W. Lv, N. Lei, Y. Zhang, X. Zhang, Y. Zhou, and W. Zhao, "Voltage controlled magnetic skyrmion motion for racetrack memory," *Sci. Rep.* **6**, 23164 (2016).
- <sup>5</sup>S. Li, W. Kang, Y. Huang, X. Zhang, Y. Zhou, and W. Zhao, "Magnetic skyrmion-based artificial neuron device," *Nanotechnology* **28**, 31LT01 (2017).
- <sup>6</sup>A. N. Bogdanov and U. K. Rößler, "Chiral symmetry breaking in magnetic thin films and multilayers," *Phys. Rev. Lett.* **87**, 037203 (2001).
- <sup>7</sup>B. Dupé, G. Bihlmayer, M. Böttcher, S. Blügel, and S. Heinze, "Engineering skyrmions in transition-metal multilayers for spintronics," *Nat. Commun.* **7**, 11779 (2016).
- <sup>8</sup>X. Zhang, J. Xia, Y. Zhou, X. Liu, H. Zhang, and M. Ezawa, "Skyrmion dynamics in a frustrated ferromagnetic film and current-induced helicity locking-unlocking transition," *Nat. Commun.* **8**, 1717 (2017).
- <sup>9</sup>A. Soumyanarayanan, M. Raju, G. A. L. Oyarce, A. K. C. Tan, M. Y. Im, A. P. Petrović, P. Ho, K. H. Khoo, M. Tran, C. K. Gan *et al.*, "Tunable room-temperature magnetic skyrmions in Ir/Fe/Co/Pt multilayers," *Nat. Mater.* **16**, 898–904 (2017).
- <sup>10</sup>D. Zhao, L. Zhang, I. A. Malik, M. Liao, W. Cui, X. Cai, C. Zheng, L. Li, X. Hu, D. Zhang *et al.*, "Observation of unconventional anomalous hall effect in epitaxial CrTe thin films," *Nano Res.* **11**, 3116–3121 (2018).
- <sup>11</sup>Y. Tokunaga, X. Z. Yu, J. S. White, H. M. Rønnow, D. Morikawa, Y. Taguchi, and Y. Tokura, "A new class of chiral materials hosting magnetic skyrmions beyond room temperature," *Nat. Commun.* **6**, 7638 (2015).
- <sup>12</sup>Z. Hou, W. Ren, B. Ding, G. Xu, Y. Wang, B. Yang, Q. Zhang, Y. Zhang, E. Liu, F. Xu *et al.*, "Observation of various and spontaneous magnetic skyrmionic bubbles at room temperature in a frustrated kagome magnet with uniaxial magnetic anisotropy," *Adv. Mater.* **29**, 1701144 (2017).
- <sup>13</sup>R. Ozawa, S. Hayami, and Y. Motome, "Zero-field skyrmions with a high topological number in itinerant magnets," *Phys. Rev. Lett.* **118**, 147205 (2017).
- <sup>14</sup>M. He, L. Peng, Z. Zhu, G. Li, J. Cai, J. Li, H. Wei, L. Gu, S. Wang, T. Zhao *et al.*, "Realization of zero-field skyrmions with high-density via electro-magnetic manipulation in Pt/Co/Ta multilayers," *Appl. Phys. Lett.* **111**, 202403 (2017).
- <sup>15</sup>J. C. Gallagher, K. Y. Meng, J. T. Brangham, H. L. Wang, B. D. Esser, D. W. McComb, and F. Y. Yang, "Robust zero-field skyrmion formation in FeGe epitaxial thin films," *Phys. Rev. Lett.* **118**, 027201 (2017).
- <sup>16</sup>S. Zhang, J. Zhang, Q. Zhang, C. Barton, V. Neu, Y. Zhao, Z. Hou, Y. Wen, C. Gong, O. Kazakova *et al.*, "Direct writing of room temperature and zero field skyrmion lattices by a scanning local magnetic field," *Appl. Phys. Lett.* **112**, 132405 (2018).
- <sup>17</sup>F. Büttner, I. Lemesch, and G. S. D. Beach, "Theory of isolated magnetic skyrmions: From fundamentals to room temperature applications," *Sci. Rep.* **8**, 4464 (2018).
- <sup>18</sup>I. D. Mayergoyz, "Mathematical models of hysteresis (invited)," *IEEE Trans. Magn.* **22**, 603–608 (1986).
- <sup>19</sup>C. R. Pike, A. P. Roberts, and K. L. Verosub, "Characterizing interactions in fine magnetic particle systems using first order reversal curves," *J. Appl. Phys.* **85**, 6660–6667 (1999).
- <sup>20</sup>C. Pike and A. Fernandez, "An investigation of magnetic reversal in submicron-scale Co dots using first order reversal curve diagrams," *J. Appl. Phys.* **85**, 6668–6676 (1999).
- <sup>21</sup>H. G. Katzgraber, F. Pázmándi, C. R. Pike, K. Liu, R. T. Scalettar, K. L. Verosub, and G. T. Zimányi, "Reversal-field memory in the hysteresis of spin glasses," *Phys. Rev. Lett.* **89**, 257202 (2002).
- <sup>22</sup>C. R. Pike, "First-order reversal-curve diagrams and reversible magnetization," *Phys. Rev. B.* **68**, 104424 (2003).
- <sup>23</sup>A. Stancu, C. Pike, L. Stoleriu, P. Postolache, and D. Cimpoesu, "Micromagnetic and preisach analysis of the first order reversal curves (FORC) diagram," *J. Appl. Phys.* **93**, 6620–6622 (2003).
- <sup>24</sup>A. P. Roberts, D. Heslop, X. Zhao, and C. R. Pike, "Understanding fine magnetic particle systems through use of first-order reversal curve diagrams," *Rev. Geophys.* **52**, 557–602 (2014).
- <sup>25</sup>J. B. Abugri, B. D. Clark, P. B. Visscher, J. Gong, and S. Gupta, "MFM and first order reversal curve (FORC) study of switching mechanism in Co<sub>25</sub>Pd<sub>75</sub> films," *J. Appl. Phys.* **126**, 013901 (2019).
- <sup>26</sup>N. K. Duong, M. Raju, A. P. Petrović, R. Tomasello, G. Finocchio, and C. Panagopoulos, "Stabilizing zero-field skyrmions in Ir/Fe/Co/Pt thin film multilayers by magnetic history control," *Appl. Phys. Lett.* **114**, 072401 (2019).
- <sup>27</sup>R. D. Desautels, L. Debeer-schmitt, S. A. Montoya, J. A. Borchers, S. G. Je, N. Tang, M. Y. Im, M. R. Fitzsimmons, E. E. Fullerton, and D. A. Gilbert, "Realization of ordered magnetic skyrmions in thin films at ambient conditions," *Phys. Rev. Mater.* **3**, 104406 (2019).
- <sup>28</sup>J. E. Davies, O. Hellwig, E. E. Fullerton, G. Denbeaux, J. B. Kortright, and K. Liu, "Magnetization reversal of Co/Pt multilayers: Microscopic origin of high-field magnetic irreversibility," *Phys. Rev. B.* **70**, 224434 (2004).
- <sup>29</sup>J. Yu, X. Qiu, Y. Wu, J. Yoon, P. Deorani, J. M. Besbas, A. Manchon, and H. Yang, "Spin orbit torques and Dzyaloshinskii-Moriya interaction in dual-interfaced Co-Ni multilayers," *Sci. Rep.* **6**, 32629 (2016).
- <sup>30</sup>W. Legrand, J. Y. Chauleau, D. Maccariello, N. Reyren, S. Collin, K. Bouzehouane, N. Jaouen, V. Cros, and A. Fert, "Hybrid chiral domain walls and skyrmions in magnetic multilayers," *Sci. Adv.* **4**, eaat0415 (2018).
- <sup>31</sup>Z. Qin, C. Jin, H. Xie, X. Li, Y. Wang, J. Cao, and Q. Liu, "Size-tunable skyrmion bubbles in Ta/CoFeB/MgO multilayers," *J. Phys. D Appl. Phys.* **51**, 425001 (2018).

- <sup>32</sup>A. P. Roberts, C. R. Pike, and K. L. Verosub, "First-order reversal curve diagrams: A new tool for characterizing the magnetic properties of natural samples," *J. Geophys. Res.* **105**, 28461–28475, <https://doi.org/10.1029/2000JB900326> (2000).
- <sup>33</sup>C. H. Henager, J. S. McCloy, P. Ramuhalli, D. J. Edwards, S. Hu, and Y. Li, "Investigation of magnetic signatures and microstructures for heat-treated ferritic/martensitic HT-9 alloy," *Acta Mater.* **61**, 3285–3296 (2013).
- <sup>34</sup>D. Roy and P. S. Anil Kumar, "Exchange spring behaviour in SrFe<sub>12</sub>O<sub>19</sub>-CoFe<sub>2</sub>O<sub>4</sub> nanocomposites," *AIP Adv.* **5**, 077137 (2015).
- <sup>35</sup>S. Kobayashi, F. Gillemot, Á. Horváth, M. Horváth, L. Almásy, Q. Tian, and A. Feoktystov, "Investigation of effects of long-term thermal aging on magnetization process in low-silloy pressure vessel steels using first-order-reversal-curves," *AIP Adv.* **7**, 056002 (2017).
- <sup>36</sup>J. Gräfe, M. Schmidt, P. Audehm, G. Schütz, and E. Goering, "Application of magneto-optical Kerr effect to first-order reversal curve measurements," *Rev. Sci. Instrum.* **85**, 023901 (2014).
- <sup>37</sup>C. I. Dobrotă and A. Stancu, "What does a first-order reversal curve diagram really mean? A study case: Array of ferromagnetic nanowires," *J. Appl. Phys.* **113**, 043928 (2013).
- <sup>38</sup>J. C. Martínez-García, M. Rivas, D. Lago-Cachón, and J. A. García, "First-order reversal curves analysis in nanocrystalline ribbons," *J. Phys. D Appl. Phys.* **47**, 015001 (2014).
- <sup>39</sup>A. P. Roberts, Q. Liu, C. J. Rowan, L. Chang, C. Carvallo, J. Torrent, and C. S. Horng, "Characterization of hematite ( $\alpha$ -Fe<sub>2</sub>O<sub>3</sub>), goethite ( $\alpha$ -FeOOH), greigite (Fe<sub>3</sub>S<sub>4</sub>), and pyrrhotite (Fe<sub>7</sub>S<sub>8</sub>) using first-order reversal curve diagrams," *J. Geophys. Res.* **111**, B12S35 (2006).